A 3D Ray-tracing Model for UHF RFID

***Abstract*—In this work, a 3-dimensional (3D) ray-tracing model is proposed. The model is specifically tailored for RFID applications by taking into account some of its unique characteristics. The proposed model can give accurate power predictions and is suitable for indoor RFID systems operating with low fade margins. The model has been verified by comparison with Method of Moments (MoM) and practical measurements. It is shown to achieve a high accuracy with significantly less computational complexity than MoM. An example application of the model is presented comparing the performance of two antennas with similar beam patterns but different axial ratio. The predicted tag detection rates (63% and 50%) are in good agreement with the experimental data (65% and 55%), showing the accuracy of the model and its improvement over previous models which are not able to handle axial ratio as accurately.**

***Index Terms*—Indoor radio communication, Radio propagation, Ray tracing, UHF measurements, UHF propagation, Radiofrequency identification**

I. Introduction

Passive ultra-high-frequency (UHF) radio frequency identification (RFID) has been increasingly popular in indoor applications such as inventory checking and indoor localization of items [1]. Due to the multipath fading of RF signals in a complex indoor environment, direct line-of-sight (LoS) signals interfere with reflected signals from walls or other reflective surfaces. When these signals are of comparable amplitudes and out of phase, signal nulls could be formed, degrading the overall coverage rate of the system. As a result, it becomes necessary to create a propagation model that can provide accurate power predictions, so that an RFID system can be properly planned to suit specific purposes

Conventional techniques to solve the power prediction problem can be classified into 3 categories: full-wave simulation, path-loss formulas and ray-tracing. For full-wave simulation, numerical analytical methods such as method of moments (MoM) or finite-difference time-domain (FDTD) are employed. With accuracy being its biggest advantage, full-wave simulation requires a large amount of memory and extensive central processing unit (CPU) time. Implementation of such a method in large simulation areas is neither practical nor necessary in most applications. Only a very limited number of works [2]–[4] have employed full-wave simulation to predict indoor radio channels.

On the other hand, path-loss (PL) formulas are a group of empirical-statistical models in which only a few parameters are needed such as the distance from the transmitter to the receiver and attenuation factors of individual walls [5]–[8]. For instance, the PL model proposed in [8] is denoted as:

$$\text{PL[dB]} = \text{PL}(d_0) + 10\alpha \log(\frac{d}{d_0}) \qquad (1)$$

where d_0 is the reference distance and α is a fixed path-loss exponent [8].

PL formulas require much less computational power than full-wave simulation. However, one drawback of applying such formulas in indoor RFID systems is that they lack spatial information and generate a smooth power-distribution which fails to include peaks and nulls caused by multi-path fading. This phenomenon is important to RFID systems in indoor environments as it determines areas over which tags can be read.

As a result, to accurately predict power distributions in an arbitrarily-defined simulation environment, a third category of techniques based on ray-tracing has been proposed and used [9]–[15].

However, to the authors' knowledge, most of the ray-tracing models in the literature are less suitable for RFID applications as detailed in Section II. Thus, the aims of this paper are:

1) to propose an improved 3D ray-tracing model tailored for UHF RFID applications, and
2) to demonstrate the model's usefulness in helping the planning of a UHF RFID system.

The rest of this paper is organised as follows: Section II presents the design of an improved 3D ray-tracing model optimised for RFID applications. Section III verifies the ray-tracing model through full-wave simulations and measurements. An example of using the proposed model is demonstrated in section IV and a conclusion is given in in section V.

II. An Improved 3D Ray-tracing Model

Ray-tracing-based propagation models have several advantages over full-wave simulations and path-loss formulas. On the one hand, the computational complexity of ray-tracing models is far below full-wave simulation, making it suitable for large-scale simulations. On the other hand, by taking reflections and transmissions into consideration, ray-tracing techniques can accurately reproduce peaks and nulls caused by multi-path fading.

However, previous models [11]–[14], [16] have focused on mobile communications with significantly larger link budgets, and hence larger length scales, often in outdoor and urban radio propagation environments. As a result, they have made some assumptions:

1) **Antenna Patterns:** radiation patterns can be defined using functions. *Only* antenna's total gain is considered in power calculations.
2) **Polarisations:** both the transmitter (Tx) and the receiver (Rx) antennas are *linearly polarised (LP)*.

3) **Orientations:** both antennas can *only be vertically or horizontally placed*.
4) **Fresnel Coefficients:** as the linearly polarised antennas are assumed to have only vertical or horizontal orientation, they are further assumed to result in *only S or P waves* when interacting with horizontal or vertical surfaces. And the Fresnel coefficients are calculated accordingly. Also, previous models do not include the thickness of reflective surfaces in the calculation of Fresnel coefficients, making power predictions inaccurate in environments surrounded by walls.
5) **Uplinks:** calculations for uplinks are not included
6) **Axial ratio:** the axial ratio (AR) is fixed in every direction for a given antenna.

Some of these assumptions are valid in long-range (outdoor) communications and simplifies the overall system complexity. However, for RFID systems operating in indoor environments with a lower link margin, these factors mentioned above are of more significance and must be considered, especially for the polarisation, AR and orientation problems. In indoor RFID applications, tag antennas are almost always linearly polarised and randomly oriented, whereas reader antennas can be either linearly or circularly polarised (CP). Besides, even for a circularly polarised antenna, its AR can vary significantly when being viewed from different directions as shown in [17], [18]. Thus, for tags placed at different directions with respect to the transmitter, the power losses caused by polarisation mismatch can be significantly different. This problem is further complicated by the reader, and especially the tag antennas' random orientations. Moreover, for passive RFID systems that employs backscatter communications, only the downlink is considered under the assumption that systems are downlink limited. With continuous improvement in tag sensitivity, the uplink calculation is becoming increasingly important. As a result, a comparison of the proposed model to those in the literature is given in table I.

TABLE I
A COMPARISON OF THE PROPOSED MODEL AND MODELS IN LITERATURE

	[11]	[12]	[16]	**The Proposed Model**
Polarisation	Single	Single	Single	Multiple
Full-wave verification	No	No	No	Yes
Wall thickness	No	No	No	Yes
Practical antenna patterns	Symmetrical patterns only	No	Unknown	Yes
Uplink calculation	Yes	No	No	Yes
Variable AR	No	No	No	Yes

A. Model Description

1) Antenna Construction: The antenna construction algorithm is defined as in algorithm 1.

In the algorithm, ${}^{c}T^{s}$ denotes the transformation matrix from spherical coordinates to Cartesian coordinates, and is defined as the inverse of ${}^{s}T^{c}$ [19]:

Algorithm 1: Antenna Construction

Input: A text file containing θ, ϕ, E_θ, E_ϕ and G_{total}
Output: An antenna pattern containing θ, ϕ, E_x, E_y, E_z, G_x, G_y and G_z
begin
  $data \leftarrow$ readtable(filename);
  assign parameters according to text file formats;
  calculate the Poynting vector for E_θ, E_ϕ;
  derive the total radiation power P_{rad};
  for $i \leftarrow 1$ **to** length *(data)* **do**
    $\begin{bmatrix} E_x(i) \\ E_y(i) \\ E_z(i) \end{bmatrix} \leftarrow {}^{c}T^{s} \cdot \begin{bmatrix} 0 \\ E_\theta(i) \\ E_\phi(i) \end{bmatrix}$
  end
  rotate θ, ϕ according to:
  $\begin{bmatrix} r' \\ \theta' \\ \phi' \end{bmatrix} \leftarrow {}^{s}T^{c} \cdot {}^{c}T^{c} \cdot {}^{c}T^{s} \cdot \begin{bmatrix} r \\ \theta \\ \phi \end{bmatrix}$;
  rotate E_x, E_y, E_z accordingly:
  $\begin{bmatrix} E_x' \\ E_y' \\ E_Z' \end{bmatrix} \leftarrow {}^{c}T^{c} \cdot \begin{bmatrix} E_x \\ E_y \\ E_Z \end{bmatrix}$;
  calculate G_x, G_y and G_z and output results
end

$$\begin{bmatrix} \sin(\theta)\cos(\phi) & \sin(\theta)\sin(\phi) & \cos(\theta) \\ \cos(\theta)\cos(\phi) & \cos(\theta)\sin(\phi) & -\sin(\theta) \\ -\sin(\phi) & \cos(\phi) & 0 \end{bmatrix}^{-1} \tag{2}$$

whereas ${}^{c}T^{c}$ denotes the rotation matrix in Cartesian coordinates. Suppose the orientation of the antenna is defined in a Cartesian array of $[\alpha\ \beta\ \gamma]$ in degrees, where α, β and γ are the rotation angle (in degrees) on the X, Y and Z axis respectively, and the order of rotation matters. The rotation matrix in Cartesian coordinates ${}^{c}T^{c}$ is defined as:

$$\begin{bmatrix} 1 & 0 & 0 \\ 0 & \cos(\alpha) & -\sin(\alpha) \\ 0 & \sin(\alpha) & \cos(\alpha) \end{bmatrix} \cdot \begin{bmatrix} \cos(\beta) & 0 & \sin(\beta) \\ 0 & 1 & 0 \\ -\sin(\beta) & 0 & \cos(\beta) \end{bmatrix} \cdot \begin{bmatrix} \cos(\gamma) & -\sin(\gamma) & 0 \\ \sin(\gamma) & \cos(\gamma) & 0 \\ 0 & 0 & 1 \end{bmatrix} \tag{3}$$

Within the algorithm, the calculation of antenna parameters is given by [20]:

$$W = \frac{|E|^2}{2Z_0} \tag{4}$$

$$U = r^2 W \tag{5}$$

$$P_{rad} = \int_0^{2\pi} \int_0^{\pi} U \sin(\theta) d\theta d\phi \tag{6}$$

$$D = \frac{4\pi U}{|P_{rad}|} \tag{7}$$

$$G = e_{cd} D \tag{8}$$

where Z_0 is the impedance of free-space, W is the Poynting vector, U is the radiation intensity, D is the directivity of the antenna and is linked with the antenna gain through the radiation efficiency e_{cd}.

Through this algorithm, an antenna with arbitrary properties can be constructed with its gains in three polarisations calculated. An example of decomposing the radiation pattern of a dipole antenna is shown in Fig. 1.

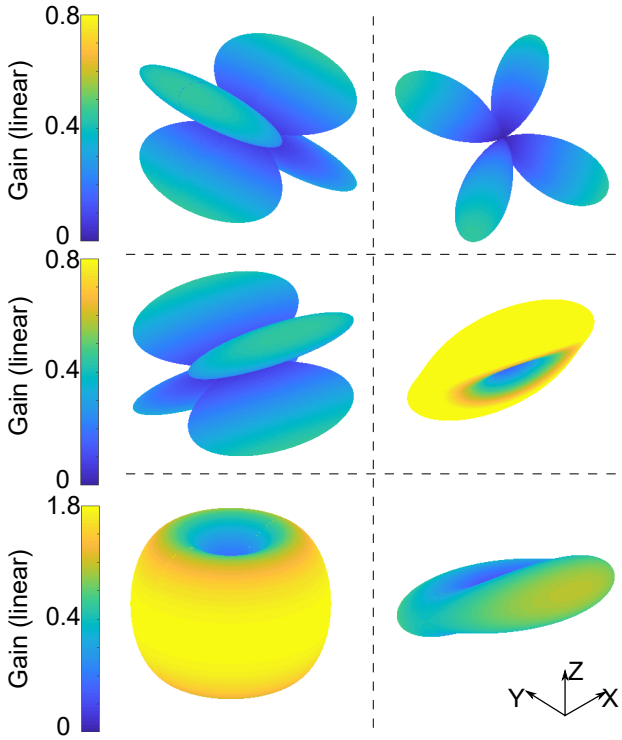

Fig. 1. First column: G_x, G_y and G_z of a vertical small dipole. Second column:G_x, G_y and G_z of the same dipole after clock-wise rotation of 45° with regard to the positive X axis. All gains are linear

2) Reflection Coefficients: Algorithm 2 calculates the Fresnel coefficients of the reflector according to the incident wave type (transverse electric, TE or transverse magnetic, TM) and the reflector properties [21]. The algorithm starts by calculating the reflection/transmission coefficients of the object and modifies these coefficients according to the thickness of the object using the recursive multi-layer model proposed in [22]. Within the algorithm, η is the complex relative permittivity defined by the operating frequency f_{GHz} and the conductivity σ [22]:

$$\eta = \varepsilon_r - 1j \cdot n^{'} \tag{9}$$

$$n^{'} = \sigma / 0.5563 / f_{GHz} \tag{10}$$

where $R^{'}$ represents the corresponding reflection coefficient (either R_{TE} or R_{TM}). The thickness model considers the interference of waves being reflected from the top and bottom layers of the material. As shown in Fig. 2, the higher a material's conductivity is, the lower this interference will be as less wave will penetrate and arrive at the bottom layer, and

Algorithm 2: Reflection Coefficients

Input: Reflector object properties

Output: Reflection and transmission coefficients R_{TE}, R_{TM}, T_{TE} and T_{TM}

begin

read object properties;

$R_{TE} \leftarrow \frac{\cos(\theta)-\sqrt{\eta-\sin^2(\theta)}}{\cos(\theta)+\sqrt{\eta-\sin^2(\theta)}}$;

$R_{TM} \leftarrow \frac{\sqrt{\eta-\sin^2(\theta)}-\eta\cos(\theta)}{\sqrt{\eta-\sin^2(\theta)}+\eta\cos(\theta)}$;

$T_{TE} \leftarrow \frac{2\cos(\theta)}{\cos(\theta)+\sqrt{\eta-\sin^2(\theta)}}$;

$T_{TM} \leftarrow \frac{2\sqrt{\eta}\cos(\theta)}{\sqrt{\eta-\sin^2(\theta)}+\eta\cos(\theta)}$;

if thickness *is* infinite **then**

return

else

$q \leftarrow \frac{2\pi d}{\lambda}\sqrt{\eta-\sin^2(\theta)}$;

$R \leftarrow \frac{R^{'}(1-\exp(-j2q))}{1-R^{'2}\exp(-j2q)}$;

$T \leftarrow \frac{(1-R^{'2})\exp(-jq)}{1-R^{'2}\exp(-j2q)}$

end

end

the reflected wave will be further attenuated as it reaches the top surface.

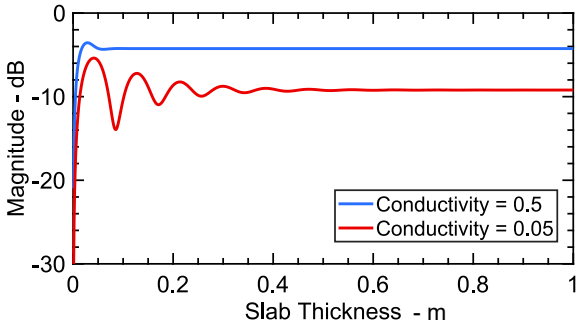

Fig. 2. The TE reflection coefficient versus layer thickness, at two different conductivities, with an incident angle of 0°

B. Power Calculation

With antenna's gain, electrical fields and reflection/transmission coefficients being calculated according to the algorithms described above, the total electric field can be calculated as the sum of all the rays.

III. Model Verification

The accuracy of the proposed ray-tracing model has been verified using a commercial Method of Moments (MoM) solver (FEKO®). It is shown that the model's result matches well with that of MoM in terms of accuracy, whereas its time

TABLE II
TIME AND MEMORY CONSUMPTION OF FEKO® AND THE PROPOSED MODEL, RUNNING THE SAME SIMULATION DESCRIBED IN THE SECTION

	Time	Memory Consumption
FEKO® with MLFMM	18.73 hours	18.10 GBytes
FEKO® with MoM	N/A	151.88 GBytes
The Proposed Model	4 seconds	6 MBytes

and memory consumption are much less. Take the following experiment as an example: a 4-by-2 metre ceiling with a thickness of 10 cm is defined 1m above the ground plane. By using standard mesh in MoM, it results in 47592 dielectric triangles and consumes a peak memory of 18.10 GBytes using multi-level fast multi-pole method (MLFMM) or 151.88 GBytes using conventional MoM, by estimation. Running on a workstation with an Intel® Core™ i7-6900K @ 3.20GHz 8-core CPU, 32 GBytes memory and an Nvidia® GTX1080 graphic card, it takes MLFMM 18.73 hours to finish all the simulation for 21 points. As a comparison, the proposed model takes less than 5 seconds and less than 6 MBytes of memory (apart from the 350 MBytes of memory used by MATLAB®, when not running the model) to run the same simulation, as shown in Table II.

In practical indoor scenarios, the composition of walls (e.g materials and layers) is much more complex than just a ground and a ceiling. This makes the difference even greater.

To further validate the model in practical applications, two scenarios are chosen and evaluated in our department building.

In these experiments, a transmitting antenna (Tx) connected with an Anritsu MG3710A signal generator [23] is placed at a certain height. The signal generator produces a signal at 860 MHz with a power of 0 dBm. To measure the power distribution, a receiving antenna (Rx) is placed at variable distances away from the Tx and the power is recorded with an Anritsu MS2690A signal analyser [24]. In total, there are six variables in the experiments:

- **Tx antenna:** a LP antenna (MT-242021NV/K [25]), a CP antenna (MT-242027/NRH/K [26]) or a wide band (WB) antenna (Poynting A-PATCH-0025 [27])
- **Rx antenna:** a LP antenna (MT-242021NV/K [25]) or a printed $\lambda/2$ dipole (PD). All TX and Rx antennas have been measured using the StarLab® antenna chamber [28].
- **Tx height (h_{Tx}):** either 1.5m or 1.1m
- **Rx height (h_{Rx}):** adjusted between 60cm and 100cm
- **Tx and Rx orientations (O_{Tx} and O_{Rx}):** varies between experiments

A. First Scenario

The first scenario is performed in the atrium of the department, and the configuration is listed in Fig. 3

A summary of the variables used in the experiments is shown in Table. III.

The wall properties used in this scenario is shown in Table. IV

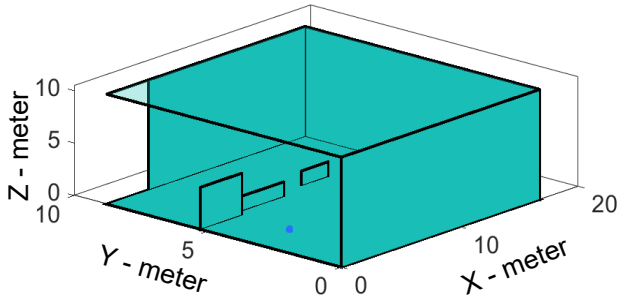

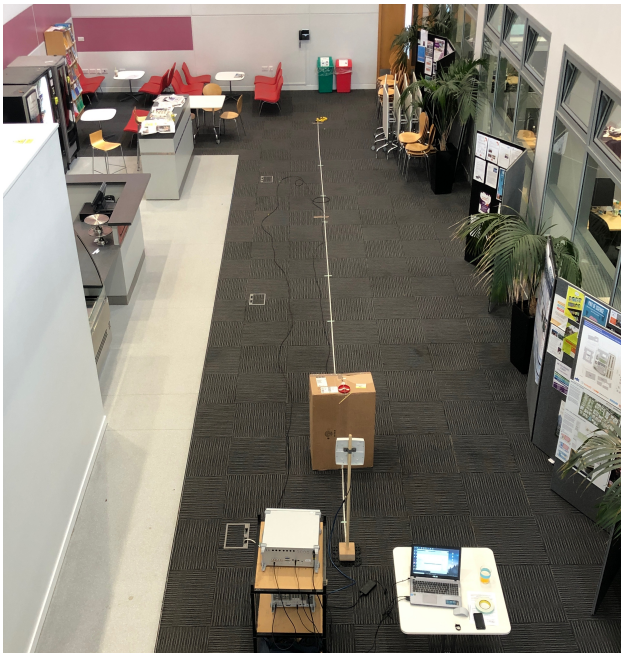

Fig. 3. Configurations of the first scenario, where the antenna is indicated by a red dot and is facing towards the positive X axis

TABLE III
CONFIGURATIONS FOR THE FIRST SCENARIO

	Tx	Rx	h_{Tx}	h_{Rx}	O_{Tx}	O_{Rx}
E1	WB	PD	1.1	0.88	$[-90\ -90\ 0\ ]$	$[0\ 0\ -90\ ]$
E2	WB	PD	1.1	0.88	$[-90\ -90\ 0\ ]$	$[0\ -135\ -90\ ]$
E3	WB	PD	1.1	0.88	$[-90\ -90\ 0\ ]$	$[0\ -45\ -90\ ]$

TABLE IV
WALL PROPERTIES USED IN THE FIRST SCENARIO

	Relative Permittivity	Conductivity - S/m	Thickness - m
Walls	6	0.001	0.12
Ground	4	0.001	Infinite
Ceiling	5.5	0.001	0.12

B. Second Scenario

The measurements for the second scenario are taken in the corridor on the first floor of the department, and the configuration is shown in Fig. 4.

A summary of the configurations used in the second scenario is shown in Table. V, whereas the wall properties used in the simulation is defined in Table. VI. It should be noticed that the ceiling of the department building is covered by a thin layer of metal foil, and thus the conductivity of the ceiling is set to be 10^7 S/m, which is a typical value for metals.

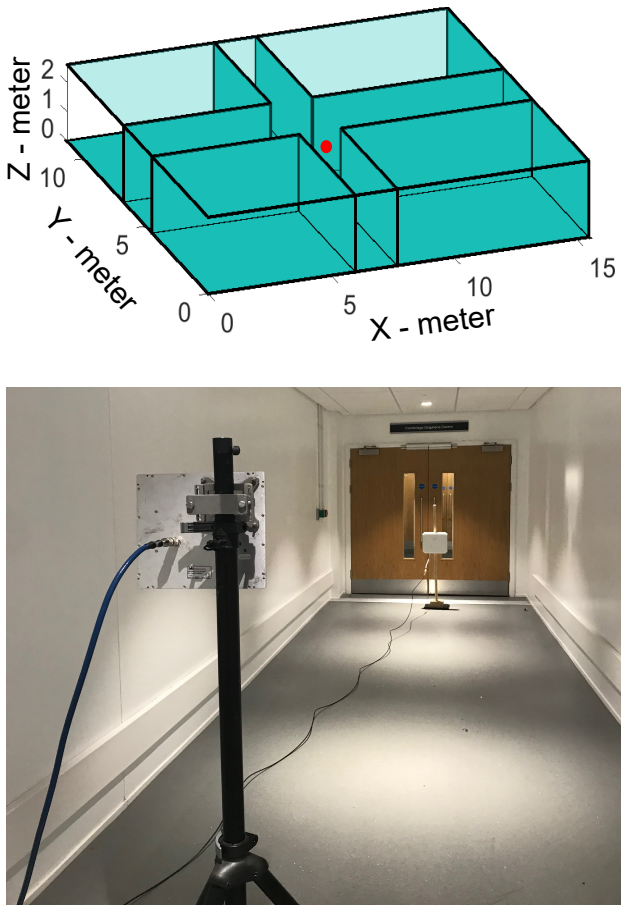

Fig. 4. Configurations of the second scenario, where the antenna is indicated by a red dot and is facing towards the positive X axis

TABLE V
CONFIGURATIONS FOR THE SECOND SCENARIO

	Tx	Rx	h_{Tx}	h_{Rx}	O_{Tx}	O_{Rx}
E1	LP	LP	1.35	0.95	[−90 −90 0]	[−90 90 0]
E2	LP	LP	1.35	0.95	[90 −90 −90]	[90 90 −90]
E3	CP	LP	1.35	0.95	[−90 −90 0]	[−90 90 0]

C. Result Analysis

The measured and simulated results of the received signal strength are shown in Fig. 5 and Fig. 6. Cumulative distribution functions (CDF) in scenario 1 are given in Fig. 5. From these results, it is clear that the proposed model can precisely reproduce the power distribution in both scenarios, even with very general wall properties being used. These wall properties can be further optimised using techniques in [29], [30] to improve accuracy.

TABLE VI
WALL PROPERTIES USED IN THE SECOND SCENARIO

	Relative Permittivity	Conductivity - S/m	Thickness - m
Walls	6	0.001	0.12
Ground	4	0.001	0.2
Ceiling	5.5	10^7	0.12

For the first scenario, within a 6 metre range the model gives very accurate predictions of the power distribution. After 6 metres, because the omni-directional receiver antenna is susceptible to multi-path effect and hence some ripples appear. Nevertheless, the model is still able to give statistically correct predictions as shown in Fig. 5.

For the second scenario, because an LP receiver antenna with a ground plane is used, the system is less sensitive to multi-path effects, resulting in a much smoother curve. Again the model gives very accurate predictions of the received power with only a few nulls slightly shifted which are most likely due to inaccuracies in the wall property definitions.

IV. AN EXAMPLE APPLICATION

In this example we experimentally verify the predictive performance of the model in terms of tag detection rate for two antennas having similar radiation patterns, but different AR.

In [18], a beam-scanning UHF reader antenna with a wide AR beamwidth is proposed, which has a unique property of changing its AR without affecting its total gain. It is shown that using the static beam configuration, the proposed antenna with an optimised AR (close to 0 dB) and a degraded AR (around 6 dB) could achieve a tag read-rate of 65% and 55% respectively. In this example, the same configuration is used as shown in Fig. 7.

The transmitting antenna is placed on the ceiling of a $3m \times 5m$ room and the transmitting power is set to be 26 dBm. With respect to the radiation patterns and AR performance of the two antennas, readers can refer to [18] for details. Two CP receiving antennas (MT-242027/NRH/K [25]) are located in the corners of the room, facing 45° downwards. 10000 observation points are evenly distributed at a height of 0.5m. At each point, we assume that two orthogonal tags are placed (oriented along the X and Y axis respectively), tags along Z axis are not considered since then the radiation nulls of the tag antennas will be facing the reader antenna which will result in poor power receptions at tags. Each tag [31] has a dipole-like radiation pattern and a sensitivity of around -17 dBm, while the reader used is based on Indy R2000 [32] which has a sensitivity of around -90 dBm. The simulation results are shown in Fig. 8. An experimental validation of the results is also carried out using 300 tags [31] which are

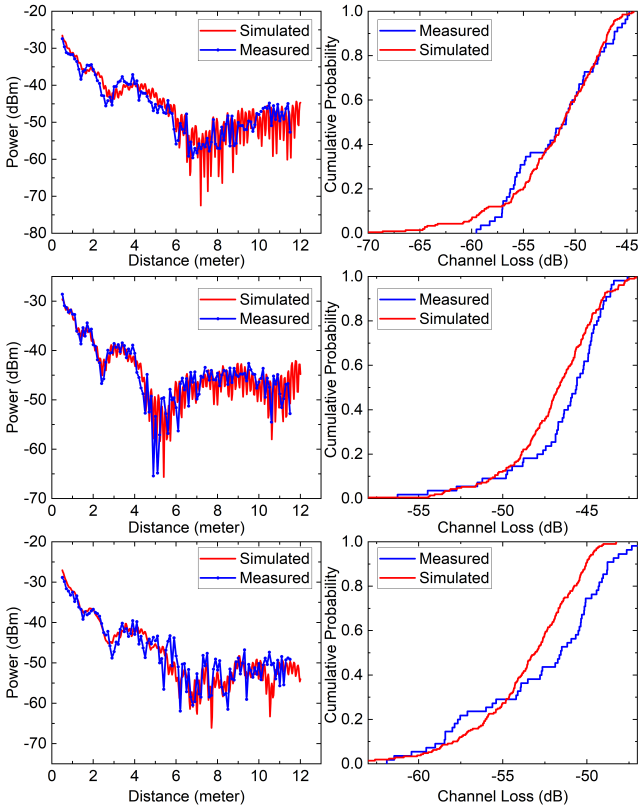

Fig. 5. Left: Measured and simulated channel loss in scenario 1, E1 to E3 (top to bottom). Right: Cumulative distribution of points with distance larger than 6 m in E1 to E3 (top to bottom).

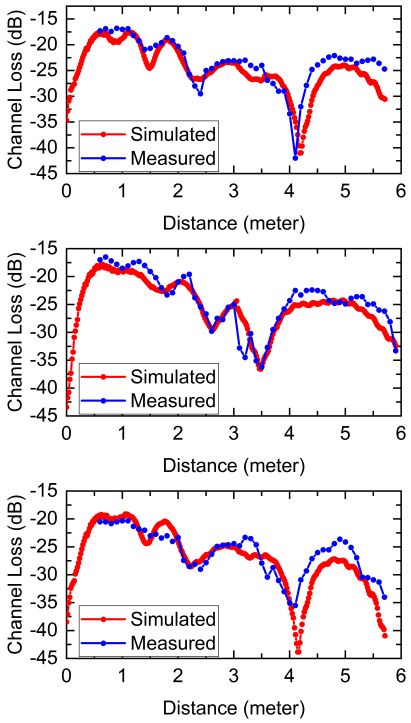

Fig. 6. Measured and simulated channel loss in scenario 2, E1 to E3 (top to bottom)

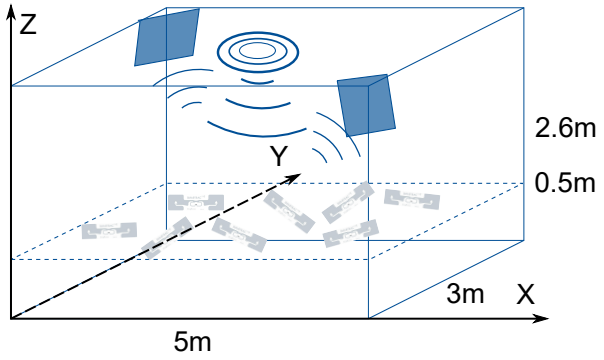

Fig. 7. The test environment [18]

randomly distributed over the area in the X and Y orientations, as detailed in [18].

We define coverage as: a tag is covered if in the downlink the received power is higher than the tag sensitivity and in the uplink the power is higher than the reader sensitivity. To achieve a successful tag detection, both conditions must be met.

From Fig. 8, we can see that although the total gain of both antennas are the same, for the AR optimised antenna, its power distribution for tags oriented along the X axis is comparatively smaller than that of the AR degraded antenna. Nevertheless it is still enough to cover the majority parts of the simulation area. Whereas in the power distribution for tags oriented along the Y direction, in general a higher power at each tag can be seen for the AR optimised antenna.

A plot of the percentage of coverage versus tag sensitivity predicted by the model is shown in Fig. 9. The coverage ratios (63% and 50%) at a -17 dBm tag sensitivity are in good agreement with the experimental data in [18] (65% and 55%). The small differences are most likely caused by the variations in the sensitivity of individual tags and/or the non-uniform distribution of their locations.

This example shows the importance of including AR performance in ray-tracing models for UHF RFID. Our model suggests that even with the same total gain, small variations in AR could result in two antennas to have different power distributions in various tag orientations and hence affect the system coverage/read rates. It also demonstrates the high accuracy and usefulness of the model which could save significant time in the planning and deployment of RFID systems.

V. Conclusion

In this paper, an improved 3D ray-tracing model tailored for RFID applications is proposed. The model is verified against a commercial MoM simulation software and practical measurements and is shown to precisely reproduce the power distribution in indoor environments. Moreover, when compared with MoM, the proposed model consumes orders

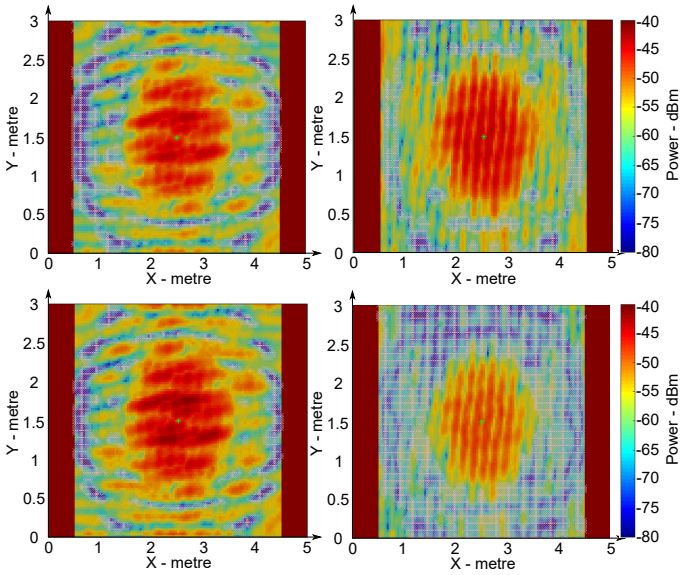

Fig. 8. Top row: results for the AR optimised antenna, bottom row: results for the AR degraded antenna. Left column: tags oriented along the X axis, right column: tags oriented along the Y axis. Downlink-limited points are marked with white crosses while uplink-limited points are marked with blue triangles (none in this plot)

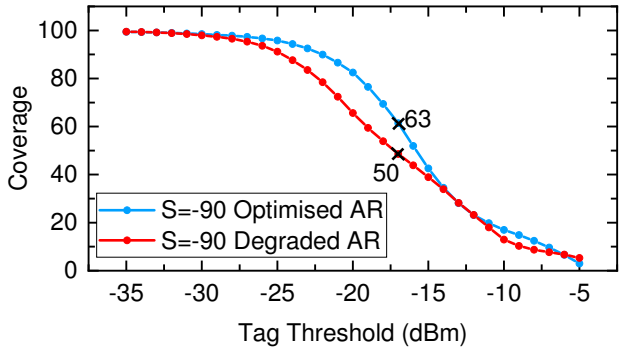

Fig. 9. Coverage vs. tag sensitivity at a reader sensitivity of -90 dBm

of magnitudes less time and memory, when the same wall configurations are being used.

An example application of the model is presented, showing that the model's unique feature allows accurate prediction of the proportion of tags detected in an example scenario involving two antennas of similar gain pattern, but different AR. The ability to make rapid, precise predictions of tag coverage will allow rapid design of RFID system deployments.

VI. Acknowledgement

This work was supported by EPSRC EP /S-19405/1 Channel Optimised Distributed Passive Sensor Networks.

References

[1] D. M. Dobkin, *The RF in RFID: UHF RFID in practice*. Newnes, 2012.

[2] Ying Wang, S. Safavi-Naeini, and S. K. Chaudhuri, "A hybrid technique based on combining ray tracing and fdtd methods for site-specific modeling of indoor radio wave propagation," *IEEE Transactions on Antennas and Propagation*, vol. 48, no. 5, pp. 743–754, May 2000.

[3] J. Lee and A. Lai, "Fdtd analysis of indoor radio propagation," in *IEEE Antennas and Propagation Society International Symposium. 1998 Digest. Antennas: Gateways to the Global Network. Held in conjunction with: USNC/URSI National Radio Science Meeting (Cat. No. 98CH36*, vol. 3. IEEE, 1998, pp. 1664–1667.

[4] K. Pahlavan and A. H. Levesque, *Wireless information networks*. John Wiley & Sons, 2005, vol. 93.

[5] A. Motley and J. Keenan, "Personal communication radio coverage in buildings at 900 mhz and 1700 mhz," *Electronics Letters*, vol. 24, no. 12, pp. 763–764, 1988.

[6] A. Motley, J. Keenan *et al.*, "Radio coverage in buildings," *Bell System Technical Journal (BTSJ)*, vol. 8, pp. 19–24, 1990.

[7] V. Degli-Esposti, G. Falciasecca, F. Fuschini, and E. Vitucci, "A meaningful indoor path-loss formula," *IEEE Antennas and Wireless Propagation Letters*, vol. 12, pp. 872–875, 2013.

[8] M. Hata, "Empirical formula for propagation loss in land mobile radio services," *IEEE transactions on Vehicular Technology*, vol. 29, no. 3, pp. 317–325, 1980.

[9] J. W. McKown and R. L. Hamilton, "Ray tracing as a design tool for radio networks," *IEEE Network*, vol. 5, no. 6, pp. 27–30, Nov 1991.

[10] Zhong Ji, Bin-Hong Li, Hao-Xing Wang, Hsing-Yi Chen, and T. K. Sarkar, "Efficient ray-tracing methods for propagation prediction for indoor wireless communications," *IEEE Antennas and Propagation Magazine*, vol. 43, no. 2, pp. 41–49, April 2001.

[11] D. Arnitz, "Tag localization in passive UHF RFID," PhD thesis, May 2011.

[12] S. Hosseinzadeh, H. Larijani, and K. Curtis, "An enhanced modified multi wall propagation model," in *2017 Global Internet of Things Summit (GIoTS)*. IEEE, 2017, pp. 1–4.

[13] J. W. Wallace, W. Ahmad, Y. Yang, R. Mehmood, and M. A. Jensen, "A comparison of indoor mimo measurements and ray-tracing at 24 and 2.55 ghz," *IEEE Transactions on Antennas and Propagation*, vol. 65, no. 12, pp. 6656–6668, Dec 2017.

[14] M. Inomata, T. Imai, K. Kitao, Y. Okumura, M. Sasaki, and Y. Takatori, "Prediction accuracy of hybrid method based on ray-tracing and effective roughness model in indoor environment for millimeter waves," in *2017 IEEE Conference on Antenna Measurements Applications (CAMA)*, Dec 2017, pp. 44–46.

[15] Y. Chen, F. Lai, and J. You, "Analysis of antenna radiation characteristics using a hybrid ray tracing algorithm for indoor wifi energy-harvesting rectennas," *IEEE Access*, vol. 7, pp. 38 833–38 846, 2019.

[16] V. Degli-Esposti, D. Guiducci, A. de'Marsi, P. Azzi, and F. Fuschini, "An advanced field prediction model including diffuse scattering," *IEEE Transactions on Antennas and Propagation*, vol. 52, no. 7, pp. 1717–1728, 2004.

[17] R. Chen, S. Yang, A. M. Ndifson, I. H. White, R. V. Penty, and M. Crisp, "A UHF RFID reader antenna with tunable axial ratio and fixed beamwidth," in *14th European Conference on Antennas and Propagation (EuCAP) 2020*. IEEE, 2020, (To be published).

[18] R. Chen, S. Yang, A. M. Ndifon, I. H. White, R. V. Penty, and M. Crisp, "Beam scanning UHF RFID reader antenna with high gain and wide axial ratio beamwidth," *IEEE Journal of Radio Frequency Identification*, 2020.

[19] Y. Rahmat-Samii, "Useful coordinate transformations for antenna applications," *IEEE Transactions on Antennas and Propagation*, vol. 27, no. 4, pp. 571–574, 1979.

[20] C. A. Balanis, *Antenna theory: analysis and design*. John wiley & sons, 2016.

[21] A. I. Lvovsky, "Fresnel equations," *Encyclopedia of Optical Engineering*, vol. 27, pp. 1–6, 2013.

[22] I. T. Union. (2015, jul) Effects of building materials and structures on radiowave propagation above about 100 MHz. Accessed on: May 5, 2019. [Online]. Available: https://www.itu.int/dms_pubrec/itu-r/rec/p/R-REC-P.2040-1-201507-I!!PDF-E.pdf

[23] Anritsu. (2019, jun) Vector signal generator mg3710a. [Online]. Available: https://www.anritsu.com/en-us/test-measurement/products/mg3710a

[24] Anritsu. (2019, jun) Signal analyzers ms2690a. [Online]. Available: https://www.anritsu.com/en-us/test-measurement/products/ms2690a

[25] M. W. E. LTD. (2019, may) MT-242021/NV/K 865 - 870 MHz, 8 dBi linear vertical polarity reader antenna. Accessed on: May 5, 2019. [Online]. Available: https://www.mtiwe.com/?CategoryID=255&ArticleID=53
[26] M. W. E. LTD. (2019, may) MT-242027/NRH/K 865 - 870 MHz, 8.5dBic RHCP reader antenna. Accessed on: May 5, 2019. [Online]. Available: https://www.mtiwe.com/?CategoryID=278&ArticleID=56
[27] Poynting. (2019, jun) Patch-25. [Online]. Available: https://poynting.tech/product/patch-25/
[28] MVG. (2019) StarLab. Accessed on: May 5, 2019. [Online]. Available: https://www.mvg-world.com/en/products/field_product_family/antenna-measurement-2/starlab
[29] D. Pena, R. Feick, H. D. Hristov, and W. Grote, "Measurement and modeling of propagation losses in brick and concrete walls for the 900-mhz band," *IEEE Transactions on Antennas and Propagation*, vol. 51, no. 1, pp. 31–39, 2003.
[30] J. Beneat and N. Bailey, "Optimization of building material properties for accurate indoor ray tracing models," in *IEEE MILCOM 2004. Military Communications Conference, 2004.*, vol. 2. IEEE, 2004, pp. 1010–1014.
[31] A. DENNISON. (2019, jun) Uhf rfid inlay: Ad-236u7. [Online]. Available: https://rfid.averydennison.com/en/home/innovation/rfid-inlay-designs/AD-236u7.html
[32] IMPINJ. (2019, oct) Indy r2000 rain rfid reader chip. [Online]. Available: https://www.impinj.com/platform/connectivity/indy-r2000/